

# On Detecting Drunk Drivers in Mixed Autonomous Platoons Using Vehicles Velocity Measurements

Abdelrahman Khalil<sup>1</sup> Khaled F. Aljanaideh<sup>2</sup> Mohammad Al Janaideh<sup>1</sup>

**Abstract**—Drunk drivers, who critically and continuously threaten road safety, are usually detected using biological sensors within the same vehicle or after drunk driving behavior is observed by police patrols. Observing an obvious drunk driving behavior indicates a relatively high blood alcohol concentration, and thus detecting drunk drivers with a relatively-low blood alcohol concentration is difficult. This study uses output-only measurements available from motion sensors in the longitudinal drive of mixed autonomous and human-driven platoons to detect drunk drivers’ behavior in human-driven vehicles within the same platoon. The human-driven vehicle is assumed to be between two autonomous vehicles that are able to share information with each other. The proposed approach relates a set of motion sensor measurements with another within the platoon and does not require knowledge of the excitation signal or the dynamics of the platoon. Numerical simulations are firstly implemented to test the proposed approach, and then VISSIM software is implemented to simulate realistic road topography. Further validations on laboratory mobile robots are presented in this paper, where a class of abnormal driving conditions that includes human-driven vehicles is simulated. Experiments are carried out by measuring abnormal human-driven vehicles within connected autonomous robots. This method is shown to deal with various system uncertainties, and the approach can deal with the drunk driver case. The drunken driving conditions are modeled mathematically with different blood alcohol concentration levels, which correspond to different effects and different drunk driving behaviors. The proposed transmissibility-based drunk driver detection algorithm is shown to detect drivers with risky, relatively low alcohol concentrations.

## I. INTRODUCTION

Drunk driving behaviors cause almost 30 deaths every day in the United States only, according to the National Highway Traffic Safety Administration (NHTSA) [1]. Moreover, around 380 deaths worldwide are caused by drunk driving every day. Drunk driving is among three main reasons for car accidents, most of them are among people aged between 16-24 years old [2]. Unfortunately, less than 1% of drunk drivers is addressed by the police [3]. According to NHTSA, blood alcohol concentration (BAC) higher than 0.08 increases the crash risk exponentially [1]. This includes difficulties to maintain lane position and braking appropriately. Such high BACs can be detected by surrounding vehicles or a simple detector on the steering wheel [4], which can prevent driving or inform the police. However, driving with  $BAC \leq 0.08$  is also risky as it results in losing the ability to perform two tasks at the same time, reduces the ability to track moving objects,

<sup>1</sup>A. Khalil and M. Al Janaideh are with the Department of Mechanical Engineering, Memorial University, St. John’s, Canada amkhali1@mun.ca, maljanaideh@mun.ca

<sup>2</sup>K. F. Aljanaideh is with the Department of Aeronautical Engineering, Jordan University of Science and Technology, Irbid, Jordan kfaljanaideh@just.edu.jo

and reduces the response to emergency driving situations. Moreover, it can affect controllers that depend on the driver behavior [5], and the driver intentions estimators as in [6]. According to the same statistics in [1], 1,878 people died in 2018 due to drunk driving conditions with BACs range from 0.01 to 0.07 g/dL. This study aims to detect on-road drunk drivers in the risky range of intoxication  $0.01 \leq BAC \leq 0.08$ , which is challenging to detect by surrounding vehicles given the current approaches.

Connected autonomous vehicles (CAV) are supplied with onboard perception sensors to smoothly coexist with the current on-road human-driven vehicles safely [7]. Human drivers are susceptible to external and internal factors, including alcohol intoxication, which results in slower response time within a vehicle [8]. A number of recent studies have proposed different techniques to detect drunk drivers. These include on-road sensors, biomedical sensors, and online parametric identification to estimate the delay in the driver’s response. In [9], the detection algorithm uses on-road sensors to monitor vehicles outside the safe/normal driving zones. This method requires sensors along roads and is not able to detect risky, relatively low alcoholic amounts where the drunk driver can still maintain the lane boundaries. On the other hand, we use the available perception sensors in autonomous vehicles only and do not require any additional cost. In [10], a mobile device receives data from the vehicle inertial sensors, then by comparing this data with pre-installed patterns on the mobile device the abnormal driving behavior is detected. The main drawback of such methods is that the detector is the driver’s mobile device, which has no access to shut down the vehicle or force the driver to stop.

Biomedical sensors are the most common way to detect drunk drivers. In [11], a pulse sensor is attached to the steering wheel to measure the driver pulses. A moving window is computed over the pulse signal to detect abnormal pulses. In [12], a transdermal sensor is used to measure BAC, the vehicle is proposed to start with a fingerprint in case of low alcohol concentration. In [13], a human breath alcohol sensor determined the blood alcohol concentration. Other methods are based on the driver’s neuromuscular dynamics as in the model in [14]. Most of these biomedical sensors have inaccuracies in estimating BAC and most vehicles are not expected to have them.

An online parametric identification method is used in [15] to obtain the delay in the driver’s response, then by comparing it with a predefined set of delays an estimate of the BAC can be estimated. Such methods are not robust against external disturbances and are difficult to count for other drunken driving conditions (i.e. short-term memory loss). In [3], a nonintrusive system has been developed to comprise inertial sensors, car

telemetry, and road lane data to detect drunk drivers. The data collected is processed through neural networks to detect abnormal driving behaviors. A similar algorithm is used in [16], [17] with deep-learning-based approach. However, the self-detection in the vehicle itself may not give a sufficient alert to the surrounding vehicles. In some cases, the lane-keeping assist systems as in [18], [19] will recover the intoxicated driver's disability to maintain the road lane, which makes it even more difficult for the surrounding vehicles to notice the drunk driver.

A number of studies in the literature investigated detecting drivers' drowsiness. In [20], the driver respiratory signals are measured and filtered to decrease the noise levels, then the filtered signals are compared with a breath-to-breath time estimation to detect drowsiness. The challenge in this mechanism is the difficulty in measuring respiratory activity, which is highly susceptible to external disturbances such as open windows and other people breathing in the car. Heart rate variability features are monitored in [21] to detect the heart rate abnormal variations based-on multivariate statistical process control. This method detects specific features but necessitates an enormous amount of statistical historical data. Camera-based techniques for detecting driver drowsiness have received a lot of attention in the literature. For example, in [22], [23] a camera-based algorithm is used to extract face features, and the scene is analyzed using deep neural networks to detect driver's drowsiness. However, unlike drowsiness, the face features of drunk drivers especially on moderate drunken levels seem normal. For example, drowsiness leads to longer blinks which can be classified as an abnormal condition, but moderate drunken levels can make the driver happy and excited, which cannot be distinguished from similar face features from normal conditions. The work in [24] investigates detecting drowsiness and drunk drivers. Camera-based eye tracking is used to detect drowsiness, but separate alcohol sensors are used to detect drunk drivers.

Techniques based on signal estimation are widely common in health monitoring and control of vehicle platoons. For example, in [25], signal estimation is implemented to count for the vehicles' bidirectional interaction that might lead to string instability, and engine saturation constraints that might lead to loss of cohesiveness. The bidirectional interaction was handled by designing bidirectional reference dynamics with proven string stability properties. Moreover, engine constraints are handled via a proposed mechanism that makes a reference that properly saturates their action. Signal estimation is used also in [26] in an adaptive protocol for synchronized merging in the cyclic communication scenario. The protocol exploits a set of adaptive control strategies, designed to cope with uncertain driveline time constants.

The proposed method takes into account that the human-driven vehicle is between two autonomous vehicles, and the two autonomous vehicles have the ability to share information with each other through V2V communication links. The autonomous vehicles can then determine whether the human drivers are normal (not drunk) or not (drunk driver). The proposed approach uses *transmissibility operators*, which are mathematical relationships between two subsets of sensor

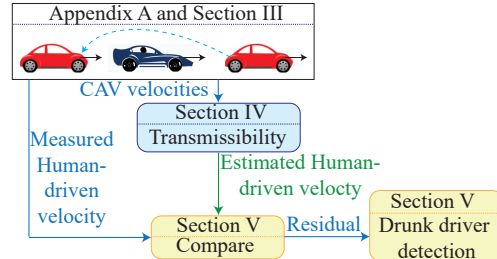


Fig. 1: A flow chart of the technical contents in this paper. The CAV velocities are used along with transmissibilities to obtain an estimation of the normal driver velocity. The drunk driver is then detected by comparing the estimated with the measured human-driven vehicle velocity. Please refer to Figure 4 for more details.

measurements of an underlying system; both the inputs and outputs of transmissibilities are outputs of the underlying system. Time-domain transmissibilities are independent of the excitation and the dynamics of the underlying system [27], [28]. Transmissibility-based health monitoring was used successfully to monitor faults in the fully connected autonomous vehicle platoon [29].

It is worth noting that the proposed method is not limited to drunk drivers and can be applied to a variety of abnormal driving behaviors. The proposed method is based on estimating a range of acceptable healthy driving conditions, and if the measured human-driver behavior falls outside of this range, it can be considered abnormal driving conditions. This includes detecting drowsiness, distracted drivers (e.g., cell phone use), drivers with health issues, or drivers with similar effects to drunkenness, such as drivers under the influence of drugs.

We begin by using the Intelligent Driver Model (IDM) as an example of good driving behavior. IDM allows to directly manipulate driver behavior such as response time and look ahead distance, allowing to study different drunken driving behaviors. Following that, the IDM is designed with three drunken driving behaviors that correspond to three different levels of intoxication. We use the bond graph model to create a numerical model for autonomous vehicles. This model simulates power propagation between different electromechanical components, allowing for a more realistic vehicle dynamics simulation. The proposed transmissibility technique is first tested with the bond graph model and the IDM model. The proposed approach is then tested on a realistic road element with curves and ramps using VISSIM software. Then, we use laboratory mobile robots to simulate a class of abnormal driving conditions that includes human-driven vehicles. Experiments are carried out to test the proposed approach by measuring abnormal human-driven vehicles within a network of connected autonomous robots. It is important to note that transmissibilities can deal with various system uncertainties, and can deal with the drunk driver case as well.

## II. CHALLENGES AND MAIN CONTRIBUTIONS

This work is motivated by the fact that CAV platoons will be supplied with adequate technology to supervise their surrounding, and thus detecting drunk drivers remains a matter of research. However, many challenges arise as follows:

- **On-road normal human-driven vehicles:** The smooth coexistence between CAVs and current on-road human-driven vehicles safely is still a challenge [7], [30]. The main problems that arise for this coexistence include the slow response of human-driven vehicles, communication with human-driven vehicles is not possible, and the problem of unknown human-driver behavior [7]. Over and above, drunken driving conditions result in even slower response and impairments in the driver behavior that is already unknown. Thus, the problem of unknown human-driver behavior plays a critical role for CAVs to distinguish drunk drivers from normal drivers.
- **External disturbances:** Road irregularities such as bad road terrains play a crucial role in detecting drunk drivers. For example, consider a road with non-smooth road terrains that prevent the vehicle from operating smoothly. In this case, the other vehicles in the platoon cannot determine whether this non-smooth performance came from an abnormal driver or from road irregularities. Other sources of disturbances play a similar role, such as weather conditions and change and road friction.
- **Various range of BAC:** Different intoxication levels result in highly different behaviors (i.e. happy-excited on one level and aggressive-anxious on another). The only effect that is shown to be proportional to the intoxication level is the slow response [1]. That is a higher BAC results in a slower driver response. This is combined with many other effects that appear on different BAC levels such as declination in visual functions, reduced ability to track moving objects, and short-term memory loss. As the BAC level is unknown by CAVs, predicting how the human-driver behavior changes under drunken driving conditions is a challenge.
- **Dynamics of CAV platoons:** The dynamics of a single CAV might be known from the manufacturer, however, CAVs platoons are constructed from any group of vehicles where each follows different dynamics. Therefore, a single CAV behavior can be predicted, but it is still a challenge to predict how each CAV will behave in platoons considering the communication links and road environment [31], [32].

Based on the problems highlighted in the literature and considering the main challenges, the main contributions of this work are as follows:

- We introduce an algorithm that uses output-only measurements available from the autonomous and human-driven vehicle sensors to detect drunk drivers. This algorithm assumes the unknown desired velocity of the platoon, unknown normal human-driven behavior, robustness against external disturbances, and unknown platoon dynamics.
- The detectors in the proposed algorithm are different from the risky agent itself, which renders avoiding drunk drivers and contacting the authorities more feasible.
- The proposed algorithm detects a relatively low concentration of alcohol due to the high estimation accuracy of the normal behavior under external disturbances and different sources of noise. This amount of alcohol is risky

and difficult to be notable by other drivers.

### III. DRUNK DRIVER MODEL

The human-driver behavior in human-driven vehicles is unknown and difficult to be predicted due to many reasons such as different driving experiences and sudden changes in decisions. The proposed approach considers unknown human-driver behavior and is independent of the human effects. However, the alterations in the driver behavior due to increasing the BAC level are known. For example, regardless of how slow or fast, the human-driver response is, increasing the BAC level in the driver's blood will always result in a slower response. The proposed approach mission is capturing (identifying) the unknown healthy human-driver behavior and then inspecting the existence of any drunkenness alterations. This section inspects the drunk driving conditions and their alterations from the healthy driver behavior. The next section shows how to capture healthy driver behavior.

#### A. Healthy Human-driver Model

The following human-driver model is an example of healthy driver behavior that will be used to show the drunkenness alterations and model the drunkenness conditions. Once again, the proposed approach considers the healthy human-driver behavior to be unknown. We take the human Intelligent Driver Model (IDM) in [33] as an example of a healthy-driver behavior, and then we alter it to the drunk driver models. The IDM model is given by

$$a_{i_H}(t, v_{i_H}) = a_{\max} \left[ 1 - \left( \frac{v_{i_H}(t)}{v_{i_H}^*(t)} \right)^\lambda - \left( \frac{s_{i_H}^*(t, v_{i_H}, \Delta v)}{s_{i_H}(t)} \right)^2 \right], \quad (1)$$

where  $a_{i_H}$  is the acceleration of the human-driven vehicle  $i_H$ ,  $a_{\max}$  is the maximum acceleration,  $v_{i_H}$  and  $v_{i_H}^*$  are the velocity of the human-driven vehicle and the desired velocity of the human-driven vehicle, respectively,  $\lambda$  is a constant that indicates how slow the human response is,  $s_{i_H}$  is the actual spacing distance between the human-driven vehicle and the vehicle in front of it, and  $s_{i_H}^*$  is the desired spacing distance and is given by

$$s_{i_H}^*(t, v_{i_H}, \Delta v) = s_0 + \max \left( 0, v_{i_H}(t)T + \frac{v_{i_H}(t)\Delta v_{i_H}(t)}{2\sqrt{a_{i_H}(t)a^*(t)}} \right), \quad (2)$$

where  $s_0$  is the minimum spacing distance,  $T$  is a time constant and  $\Delta v(t)$  is the velocity difference between the vehicle  $v_{i_H}$  and its preceding vehicle  $v_{i_H-1}$ , and  $a^*$  is the desired acceleration.

#### B. Drunkenness Driving Conditions

In this section, we introduce the drunkenness alterations in the normal human drivers due to increasing the BAC to different levels. The following alterations are related to the BAC levels and the drunken driving conditions and are independent of the healthy driver behavior. For clarification purposes only, these alterations are applied to the healthy

TABLE I: Drunk driving conditions according to the alcohol concentration and the corresponding mathematical models.

BAC (g/dL)	Effects on driving	Mathematical model
0.02	1) Decline in visual functions 2) Decline in ability to perform two tasks at the same time	$\tilde{s}_{i_H}^*(t) = s_{i_H}^*(t) + \delta_{s*}(t)$ $\lambda = 3$
0.05	1) Reduced coordination 2) Reduced ability to track moving objects 3) Reduced response to emergencies	$\tilde{s}_{i_H}(t) = s_{i_H}(t) + \delta_s(t)$ $\tilde{v}_{i_H-1}(t) = v_{i_H-1}(t - t_v)$ $\lambda = 2$
0.08	1) Short-term memory loss 2) Poor speed control 3) Impaired perception 4) Reduced information processing capability	$\tilde{v}_{i_H-1}(t) = v_{i_H-1}(t) + \delta_{i_H-1}(t)$ $\tilde{v}_{i_H}(t) = v_{i_H}(t) + \delta_{i_H}(t)$ $\tilde{s}_{i_H}(t) = s_{i_H}(t - t_s)$ $\lambda = 1$



Fig. 2: Connected autonomous vehicle platoon with vehicle  $i_H$  is human-driven. The vehicle  $i_H+1$  receives the velocity  $v_{i_H-1}$  through a V2V communication link, and measures the velocity  $v_{i_H}$  through perception sensors.

driver model example introduced in section III-A. The BAC levels range from relatively low to relatively high and are shown to have different effects on each level. This drunk driver model is then used to test the drunk driver detection algorithm in section V.

Increasing the BAC level results in several effects on the driving conditions, as listed in Table I [1]. For  $BAC > 0.08g/dL$  the drunk driving behavior, which includes the inability to maintain lane boundaries or brake inappropriately, is notable by other drivers. In this paper, we focus on moderate intoxication levels  $0.02 \leq BAC \leq 0.08$ .

Let  $\tilde{s}_{i_H}^*$ ,  $\tilde{s}_{i_H}$ ,  $\tilde{v}_{i_H}$ , and  $\tilde{v}_{i_H-1}$ , denote the corrupted measurements of  $s_{i_H}^*$ ,  $s_{i_H}$ ,  $v_{i_H}$ , and  $v_{i_H-1}$ , respectively. Moreover, let  $\delta_{s*}$ ,  $\delta_s$ ,  $\delta_{i_H}$ , and  $\delta_{i_H-1}$ , be the corruptions in the measurements of  $\tilde{s}_{i_H}^*$ ,  $s_{i_H}$ ,  $v_{i_H}$ , and  $v_{i_H-1}$ , respectively. For BAC value of around  $0.02g/dL$ , a decline in visual functions arises, which we model as inaccuracies added to the desired spacing distance, that is,  $\tilde{s}_{i_H}^*(t) = s_{i_H}^*(t) + \delta_{s*}(t)$ . Losing the ability to perform two tasks at the same time (i.e. tracking the vehicle ahead and following the road signs) leads to a delay in one task to perform the other, which is modeled as a slight delay in the drivers response  $\lambda = 3$ . At  $BAC = 0.02g/dL$ , the driver model in (1) becomes

$$\tilde{a}_{i_H}(t, v_{i_H}) = a_{\max} \left[ 1 - \left( \frac{v_{i_H}(t)}{v_{i_H}^*(t)} \right)^3 - \left( \frac{\tilde{s}_{i_H}^*(t, v_{i_H}, \Delta v)}{s_{i_H}(t)} \right)^2 \right]. \quad (3)$$

For BAC levels around  $0.05g/dL$ , the reduced coordination effect is modeled as inaccuracies added to the vehicle position  $\tilde{s}_{i_H}(t) = s_{i_H}(t) + \delta_s(t)$ . The main moving object that the human-driver is expected to track is the front vehicle, we model this effect as a time delay in the velocity of the front vehicle, that is,  $\tilde{v}_{i_H-1}(t) = v_{i_H-1}(t - t_{i_H})$ . Moreover, the drunk driver loses the ability to respond to emergencies such as sudden brake which produces a slower response such that

$\lambda = 2$ . Thus, (3) becomes

$$\tilde{a}_{i_H}(t, v_{i_H}) = a_{\max} \left[ 1 - \left( \frac{v_{i_H}(t)}{v_{i_H-1}(t - t_v)} \right)^2 - \left( \frac{\tilde{s}_{i_H}^*(t, v_{i_H}, \Delta v)}{\tilde{s}_{i_H}(t)} \right)^2 \right]. \quad (4)$$

For BAC around  $0.08g/dL$ , losing the short-term memory is modelled as inaccuracies added to the front vehicle velocity  $\tilde{v}_{i_H-1}(t) = v_{i_H-1}(t) + \delta_{i_H-1}(t)$ . The poor speed control prevents the drunk driver to maintain an accurate speed for the vehicle, we model this effect as inaccuracies added to the vehicle velocity  $\tilde{v}_{i_H}(t) = v_{i_H}(t) + \delta_{i_H}(t)$ . The impaired perception is modelled as losing the ability to maintain the vehicle position within the platoon  $\tilde{s}_{i_H}(t) = s_{i_H}(t - t_s)$ . The reduced information processing capability results in an even slower response, such as  $\lambda = 1$  can be used. Thus, the drunk driver model in (4) becomes

$$\tilde{a}_{i_H}(t, v_{i_H}) = a_{\max} \left[ 1 - \left( \frac{\tilde{v}_{i_H}(t)}{\tilde{v}_{i_H-1}(t - t_v)} \right) - \left( \frac{\tilde{s}_{i_H}^*(t, v_{i_H}, \Delta v)}{\tilde{s}_{i_H}(t - t_s)} \right)^2 \right]. \quad (5)$$

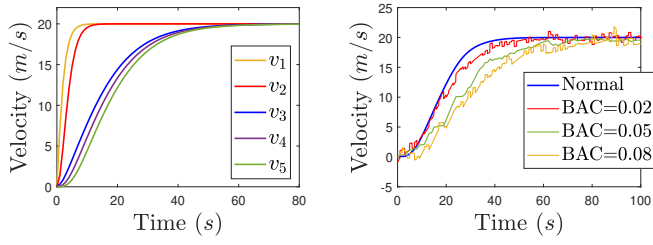
Therefore, the driver model in (A.7) can be written as

$$\tilde{a}_{i_H}(t, x_{i_H}) = \tilde{A}_{i_H} x_{i_H}(t) + \tilde{B}_{i_H} C_{i_H-1} x_{i_H-1}(t) + \tilde{f}(t, x), \quad (6)$$

where  $\tilde{A}_{i_H}$ ,  $\tilde{B}_{i_H}$ , and  $\tilde{f}$  characterize the human-driver model with  $A_{i_H}$ ,  $B_{i_H}$ , and  $f$  while the driver is drunk.

*Example 3.1:* This example simulates the healthy and drunken driving conditions of a five vehicles platoon, where all vehicles are CAVs except the third vehicle that is human-driven. All CAVs are set to follow the model in Appendix A. We consider the platoon model in (7), (8) with the parameters shown in Table A.1. Figure 3a shows the step responses of a healthy platoon with five vehicles, where the third vehicle is human-driven. Note that the human-driven vehicle takes a longer time to reach the desired velocity due to the human reaction. Next, we introduce the simulation of the drunk driver effects for  $BAC = 0.02, 0.05$ , and  $0.08 g/dL$  separately. A band-limited white noise with a signal-to-noise ratio (SNR) of 10 is set to  $\delta_{s*}$ ,  $\delta_s$ ,  $\delta_{i_H-1}$ , and  $\delta_{i_H}$ . Moreover, we set the position and velocity signals delay to  $t_v = t_s = 1$  second, and the human response time coefficient  $\lambda$  as specified in Table I. Figure 3b compares the responses of the simulated drunk driver with different alcohol concentrations. Note that increas-

ing the BAC level results in even slower human reactions.



(a) Healthy platoon with a human-driven vehicle.  
(b) Platoon with simulated model of a drunk driver.

Fig. 3: Examples 3.1: (a) Step responses of five vehicles of a healthy platoon, where the vehicle  $j = 3$  is human-driven, and (b) a comparison between human-driver step responses for healthy and simulated drunk drivers.

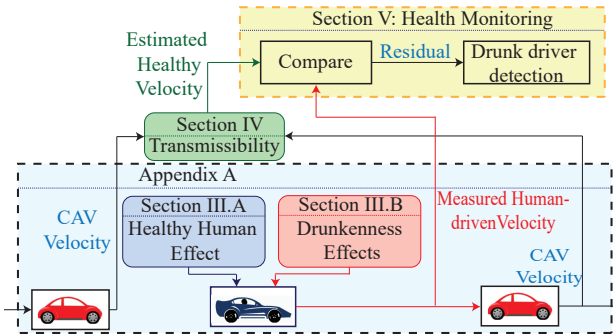


Fig. 4: The proposed transmissibility-based drunk driver detection algorithm is depicted as a block diagram on a three-vehicle platoon portion. The middle vehicle is driven by a human, while the other two are CAVs. The velocities of the CAVs are used in the transmissibility to estimate the healthy velocity of the human-driven vehicle. When the measured and estimated velocities are compared, it is possible to determine whether or not the driver is drunk.

#### IV. TRANSMISSIBILITY IDENTIFICATION OF CAV

Transmissibility operators are mathematical objects that characterize the relationship between outputs of an underlying system. In this section, we show how to identify transmissibilities between available sensor measurements in the platoon. Then, transmissibilities identified under normal driving conditions can be used to detect drunk drivers as we show in section VII.

##### A. CAV Transmissibility Operators

Consider the platoon described by the following state space model

$$\dot{x}(t) = Ax(t) + B_v v_1^*(t) + B_f f(t, x) + B_w w(t), \quad (7)$$

$$y(t) = Cx(t), \quad (8)$$

where  $A \in \mathbb{R}^{n \times n}$  is Hurwitz,  $B_v \in \mathbb{R}^{n \times (m-2)}$ ,  $B_f \in \mathbb{R}^{n \times 1}$ ,  $B_w \in \mathbb{R}^{n \times 1}$ ,  $C \in \mathbb{R}^{n \times n}$ ,  $n$  is the model order,  $n \geq 2$  is the number of vehicles,  $m$  is the number of independent excitations (inputs) on the system,  $f(\cdot, \cdot)$  is bounded unknown dynamics that includes the nonlinearizable human

effects,  $w$  is a combination of bounded uncertain dynamics and bounded unknown external disturbances (process noise),  $y(t) = [v_1(t) \dots v_n(t)]^T$ , and for  $j = 1, \dots, n$ ,  $v_j$  is the velocity of the  $j$ th vehicle. Then, define

$$y_i(t) \triangleq \begin{bmatrix} v_{i-1}(t) \\ v_{i+1}(t) \end{bmatrix} = C_i x(t) \in \mathbb{R}^p, \quad (9)$$

$$y_o(t) \triangleq v_{i_H}(t) = C_o x(t) \in \mathbb{R}, \quad (10)$$

to be two independent sets of noise-free velocity outputs, where  $p = 2$  is the number of independent pseudo inputs,

$$C_i = \begin{bmatrix} 0 & \dots & 0 & C_{i-1} & 0 & 0 & 0 & \dots & 0 \end{bmatrix},$$

$$C_o = \begin{bmatrix} 0 & \dots & 0 & C_{i_H} & 0 & \dots & 0 \end{bmatrix},$$

$$C_i \in \mathbb{R}^{p \times n} \text{ and } C_o \in \mathbb{R}^{1 \times n}.$$

**Remark 1.** In case of two or more consecutive human-driven vehicles within the same platoon, the drunk driver can still be detected by setting  $y_i$  to the velocities of the two CAVs before and after the human-driven vehicles, and  $y_o$  to the velocity of the last human-driven vehicle.

For clarification and to focus on the transmissibility concept, the definition of  $y_i$  and  $y_o$  in (9)-(10) considers only one human-driven vehicle between two CAVs. In case of two or more consecutive human-driven vehicles, same procedure can be followed after defining  $y_i$  and  $y_o$  as in **Remark 1**. This case is further discussed and experimental results are given in Section VIII.

The relationships between  $y_i$  and  $u$  and  $y_o$  and  $u$  can be written as

$$\delta(\mathbf{p})y_i(t) = \Gamma_i(\mathbf{p})u(t), \quad (11)$$

$$\delta(\mathbf{p})y_o(t) = \Gamma_o(\mathbf{p})u(t), \quad (12)$$

respectively, where

$$\Gamma_i(\mathbf{p}) \triangleq C_i \text{adj}(\mathbf{p}\mathbf{I}_n - A)B \in \mathbb{R}^{p \times p}[\mathbf{p}], \quad (13)$$

$$\Gamma_o(\mathbf{p}) \triangleq C_o \text{adj}(\mathbf{p}\mathbf{I}_n - A)B \in \mathbb{R}^{(n-p) \times p}[\mathbf{p}], \quad (14)$$

$$\delta(\mathbf{p}) \triangleq \det(\mathbf{p}\mathbf{I}_n - A), \quad (15)$$

$$u(t) = [v_1^*(t) \ f(t, x) \ w(t)]^T, \quad (16)$$

$B = [B_v \ B_f \ B_w]$ . Multiplying (11) by  $\text{adj}\Gamma_i(\mathbf{p})$  from the left and using the fact that

$$\text{adj}\Gamma_i(\mathbf{p})\Gamma_i(\mathbf{p}) = \det\Gamma_i(\mathbf{p})\mathbf{I}_n \quad (17)$$

yields

$$\delta(\mathbf{p})\text{adj}\Gamma_i(\mathbf{p})y_i(t) = \det\Gamma_i(\mathbf{p})u(t), \quad (18)$$

where  $\text{adj}\Gamma_i$  denotes the adjugate matrix of  $\Gamma_i$  and  $\mathbf{I}_n$  is the  $n \times n$  identity matrix. Moreover, multiplying (12) by  $\det\Gamma_i(\mathbf{p})$  yields

$$\delta(\mathbf{p})\det\Gamma_i(\mathbf{p})y_o(t) = \Gamma_o(\mathbf{p})\det\Gamma_i(\mathbf{p})u(t). \quad (19)$$

Next, substituting the left-hand side of (18) in (19) yields

$$\delta(\mathbf{p})\det\Gamma_i(\mathbf{p})y_o(t) = \delta(\mathbf{p})\Gamma_o(\mathbf{p})\text{adj}\Gamma_i(\mathbf{p})y_i(t). \quad (20)$$

Then the transmissibility whose pseudo input is  $y_i$  and whose

pseudo output is  $y_o$  satisfies [27]

$$y_o(t) = \mathcal{T}(\mathbf{p})y_i(t), \quad (21)$$

where

$$\mathcal{T}(\mathbf{p}) \triangleq \frac{\delta(\mathbf{p})}{\delta(\mathbf{p})}\Gamma_o(\mathbf{p})\text{adj}\Gamma_i^{-1}(\mathbf{p}), \quad (22)$$

Note that (21) is a compact way of writing the differential equation (20).

Cancellation of the common term  $\delta(\mathbf{p})$  in (20) does not exclude any solutions of the differential equation (20), and thus is allowed. This cancellation yields a reduced-order transmissibility operator. Although this result may seem straightforward to the reader, the proof has many technical details [27].

After cancelling the common term  $\delta(\mathbf{p})$ , (20) becomes

$$\det \Gamma_i(\mathbf{p})y_o(t) = \Gamma_o(\mathbf{p})\text{adj}\Gamma_i(\mathbf{p})y_i(t), \quad (23)$$

which can be written as (21) with  $\mathcal{T}$  in (22) redefined as

$$\mathcal{T}(\mathbf{p}) \triangleq \Gamma_o(\mathbf{p})\Gamma_i^{-1}(\mathbf{p}). \quad (24)$$

It is important to mention that the transmissibility operator  $\mathcal{T}(\mathbf{p})$  in (24) is independent of the excitation signals  $u$ , the initial condition  $x(0)$ , and the platoon dynamics  $\delta(\mathbf{p})$ . The next section introduces an algorithm to identify the platoon transmissibilities if the platoon model is unknown. The following identification algorithm is discrete since the platoon velocities are measured in discrete time, we transform transmissibilities to discrete time as well. Following [34], transmissibilities are transformed to discrete time by replacing  $\mathbf{p}$  in (22) with the forward shift operator  $\mathbf{q}$ .

### B. Identification of transmissibilities

Replacing  $\mathbf{p}$  in (21) with  $\mathbf{q}$  yields, for all  $k \geq 0$ ,

$$y_o(k) = \mathcal{T}(\mathbf{q})y_i(k), \quad (25)$$

where

$$\mathcal{T}(\mathbf{q}) = \Gamma_o(\mathbf{q})\Gamma_i^{-1}(\mathbf{q}) \quad (26)$$

$$= \frac{1}{\det \Gamma_i(\mathbf{q})}\Gamma_o(\mathbf{q})\text{adj}\Gamma_i(\mathbf{q}). \quad (27)$$

Transmissibility characteristics can be observed from equation (26). The zeros of  $\Gamma_i$  will shape like pseudo poles of the operator  $\mathcal{T}$ . An unstable (nonminimum phase) zero in  $\Gamma_i$  will render  $\mathcal{T}$  unstable. If  $\Gamma_i$  has less zeros than  $\Gamma_o$ , then  $\mathcal{T}$  is noncausal. Thus the identified model of  $\mathcal{T}$  must be able to deal with these instabilities and noncausalities. A third challenge faced by identifying  $\mathcal{T}$  is the unknown order since the platoon dynamics are unknown. To this end and following [35], we assume  $\mathcal{T}$  to have a model structure of a noncausal Finite Impulse Response (FIR) model that is given by

$$\mathcal{T}(\mathbf{q}, \Theta_{r,d}^{\text{FIR}}) = \sum_{i=-d}^r H_i \mathbf{q}^{-i}, \quad (28)$$

where  $r, d$  are causal and noncausal orders of the FIR model structure, respectively,  $H_i \in \mathbb{R}^{(n-p) \times p}$  is the  $i$ th coefficient of the FIR model structure, which also represents the  $i$ th Markov

parameter of the FIR model, and  $\Theta_{r,d}^{\text{FIR}} \triangleq [H_{-d}, \dots, H_r]^T$ . Next, the FIR model coefficients  $\Theta_{r,d}^{\text{FIR}}$  can be estimated based on minimizing the mean squared error (least squares) from

$$\hat{\Theta}_{r,d,\ell}^{\text{FIR}} = (\Phi_{r,d,\ell} \Phi_{r,d,\ell}^T)^{-1} \Phi_{r,d,\ell} \Psi_{v_o,\ell}, \quad (29)$$

where  $\ell$  is the number of samples,

$$\Psi_{y_o,\ell} \triangleq [y_o(r) \ \dots \ y_o(\ell-d)]^T, \quad (30)$$

$$\Phi_{r,d,\ell} \triangleq [\phi_{r,d}(r) \ \dots \ \phi_{r,d}(\ell-d)], \quad (31)$$

$$\phi_{r,d}(k) \triangleq [y_i(k+d) \ \dots \ y_i(k-r)]^T. \quad (32)$$

Note that  $\hat{\Theta}_{r,d,\ell}^{\text{FIR}} = [\hat{H}_{-d,\ell}, \dots, \hat{H}_{r,\ell}]^T$ .

## V. DRUNK DRIVER DETECTION

The proposed drunk driver detection algorithm is briefly illustrated in Figure 4. The proposed drunk driver detection uses of CAVs' velocities along with the transmissibility relations  $T$  to estimate the human-driven vehicle's velocity in the mixed platoon. Define the residual between the measured human-driven vehicle's velocity from the following CAV, and its transmissibility-based estimation at time step  $k$  as

$$e(k|\hat{\Theta}_{r,d,\ell}^{\text{FIR}}) \triangleq y_o(k) - \hat{y}_o(k|\hat{\Theta}_{r,d,\ell}^{\text{FIR}}), \quad (33)$$

where

$$\hat{y}_o(k|\hat{\Theta}_{r,d,\ell}^{\text{FIR}}) \triangleq \mathcal{T}(\mathbf{q}, \hat{\Theta}_{r,d,\ell}^{\text{FIR}})y_i(k) \quad (34)$$

The estimation of the normal human-driven vehicle's velocity  $\hat{y}_o$  will be closed to the measured human-driven vehicle's velocity  $y_o$  if the driver's behavior is normal. Abnormalities in the driver's behavior will result in discrepancies between the measured and estimated human-driven vehicle's velocity, and thus higher residual  $e$ . The detection algorithm depends on the level of these discrepancies between the estimated and measured velocities. Hence, we define our detector as the norm of residual over a sliding window with width  $w$  steps. For all  $k \geq d$ , compute

$$E(k|\hat{\Theta}_{r,d}^{\text{FIR}}, w) \triangleq \sqrt{\sum_{i=k}^{w+k} \|e(i|\hat{\Theta}_{r,d,\ell}^{\text{FIR}})\|^2}. \quad (35)$$

The definition of  $E(k|\hat{\Theta}_{r,d}^{\text{FIR}}, w)$  provides robustness against false alarms due to excessive noise at some time samples. The higher  $w$  is, the more robust  $E(k|\hat{\Theta}_{r,d}^{\text{FIR}}, w)$  is against false alarms. However, the norm of residual is computed at time step  $k$  between the steps  $k-w$  and  $k$ , which means more steps are required at each  $k$ . The acceptable range of the healthy driver's behavior is defined by defining a threshold limit on  $E(k|\hat{\Theta}_{r,d}^{\text{FIR}}, w)$ . Assume the driver to be healthy for the first  $M$  steps, where  $M \geq w+d$ , then define the threshold [36]

$$\mu(\hat{\Theta}_{r,d,\ell}^{\text{FIR}}, w, M) \triangleq \frac{\eta}{M+1} \sum_{i=d}^M E(i|\hat{\Theta}_{r,d,\ell}^{\text{FIR}}, w), \quad (36)$$

where  $\eta$  is the acceptable signal-to-noise ratio,

TABLE II: The identified transmissibility operators used to detect drunk drivers from each pseudo input to the human-driven output  $v_3$ .

Operator	Pseudo inputs	Pseudo output
$\mathcal{T}_1$	$v_2, v_4$	$v_3$
$\mathcal{T}_2$	$v_1, v_4$	$v_3$
$\mathcal{T}_3$	$v_2, v_5$	$v_3$
$\mathcal{T}_4$	$v_1, v_5$	$v_3$

## VI. SIMULATION RESULTS

### A. Numerical Results Based-on Mathematical Models

This section tests the proposed approach numerically using the bond graph model in Appendix A. We construct a five vehicles mixed platoon, where the third is human-driven and the rest are autonomous. The autonomous vehicles follow the model in Figure A.1, which is interpreted in equation (A.1) along with the parameters in Table A.1. The human-driven vehicle follows the IDM model in (1)-(2). The platoon is set to move randomly by setting the desired velocity of the first vehicle to Gaussian noise as well as the external disturbances. We first run the platoon model under healthy conditions, and then implement the transmissibility identification introduced in Section IV-B. The identified parameters  $\hat{\Theta}_{r,d}^{\text{FIR}}$  (Markov parameters) of the transmissibility operator that relates the output subset  $v_2, v_4$  to  $v_3$  are plotted in Figure 5a. To validate the identified transmissibility first before implementing the drunk driver detection, we use the identified parameters in Figure 5a along with the measurements of  $v_2, v_4$  to estimate  $v_3$  while the platoon moves randomly. The measured velocity  $v_3$  and its transmissibility-based estimation  $\hat{v}_3$  are plotted in Figure 5b. For further testing, we identify the transmissibility operators defined in Table II on the same way that is introduced in Section IV-B.

Next, we introduce the simulated drunk driver effects for  $\text{BAC} = 0.02, 0.05$ , and  $0.08$  separately by setting  $\delta_{s^*}, \delta_s, \delta_{i_H-1}$ , and  $\delta_{i_H}$  to band limited white noise with a signal-to-noise ratio (SNR) of 10, and  $t_v = t_s = 1$  second. The driver response time coefficient  $\lambda$  is set to 3, 2, and 1 for  $\text{BAC} = 0.02, 0.05$ , and  $0.08$ , respectively. To observe the norm of residuals, we compute  $E$  using (35) with  $w = 100$  samples for all operators in Table II as shown in Figure 6

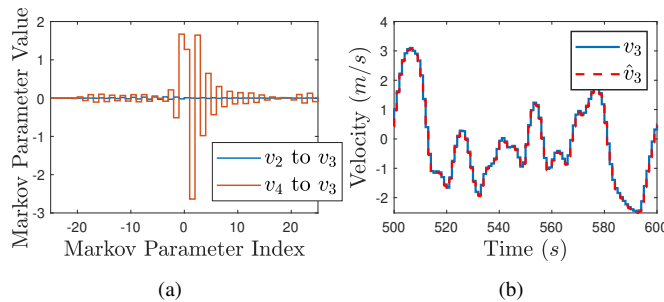


Fig. 5: Simulation results: (a) The identified parameters  $\hat{\Theta}_{r,d}^{\text{FIR}}$  (Markov parameters) of the transmissibility operator that relates the output subset  $v_2, v_4$  to  $v_3$ , and (b) A comparison between the measurements of the velocity  $v_3$  and its transmissibility-based estimation  $\hat{v}_3$ . The simulated output velocity of the third vehicle  $v_3$  and the predicted output velocity  $\hat{v}_3$ . The estimation of  $\hat{v}_3$  is obtained by implementing the identified transmissibility parameters in Figure 5a along with the measurements of  $v_2$  and  $v_4$ .

TABLE III: Simulated drunk driving conditions in VISSIM software with the corresponding blood alcohol concentration.

BAC ( $g/dL$ )	Look ahead distance	Look back distance	Lack of attention	Distr-action	Reaction time
0.00 (Normal)	250m	150m	0.0%	0.0%	1.2s
0.02	220m	120m	15%	15%	1.5s
0.05	190m	90m	25%	25%	1.8s
0.08	160m	60m	35%	35%	2.3s

along with their thresholds using (36). The jump in the level of the norm of residuals above the threshold limits in Figure 6 indicates that abnormal driving conditions are detected.

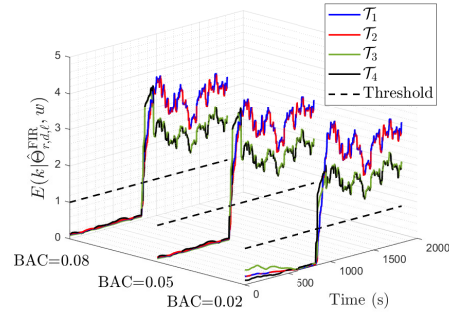


Fig. 6: Simulation results: Norm of the residuals of the transmissibilities  $\mathcal{T}_1, \dots, \mathcal{T}_4$  computed using (35) with  $w = 100$  steps. The jump in the level of  $E$  above the threshold limits around time  $t = 800$  seconds indicates that abnormal driving conditions are detected.

### B. Simulation Results using VISSIM Software

This section considers simulating more realistic road topographies using VISSIM software. VISSIM software simulates realistic roads based on 3D satellites maps, and uses statistical data to generate stochastic vehicle flows on these roads. We tested the proposed approach on the road shown in Figure 7, which is a portion of Transit Canada Highway that is located near St. John's, Canada. The testing portion starts with a slightly curved road, then an upward ramp to cross a bridge intersection, and then a downward ramp after the bridge.

We simulated a platoon with five vehicles where the third vehicle is human-driven. The desired velocity of the platoon is set to  $10m/s$ . The platoon takes around 100 seconds to cross the road portion which is with a length of  $1km$ . We first set the healthy human driver behavior to the normal

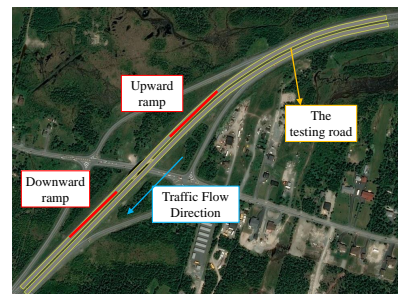


Fig. 7: A realistic road element simulated using Vissim software. This road was simulated to test the proposed approach with roads ramps and curves.

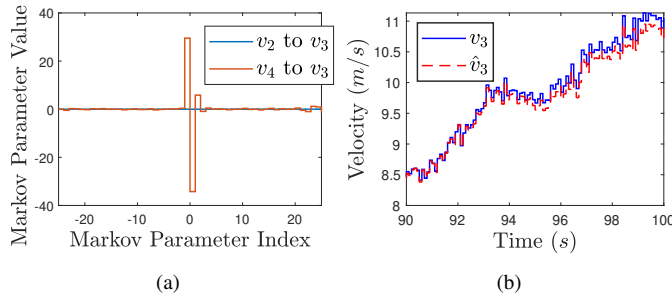


Fig. 8: VISSIM simulation results: (a) The identified parameters  $\hat{\Theta}_{r,d}^{\text{FIR}}$  (Markov parameters) of the transmissibility operator that relates the output subset  $v_2, v_4$  to  $v_3$ , and (b) A comparison between the measurements of the velocity  $v_3$  and its transmissibility-based estimation  $\hat{v}_3$ . The estimation of  $\hat{v}_3$  is obtained by implementing the identified transmissibility parameters in Figure 8a along with the measurements of  $v_2$  and  $v_4$ .

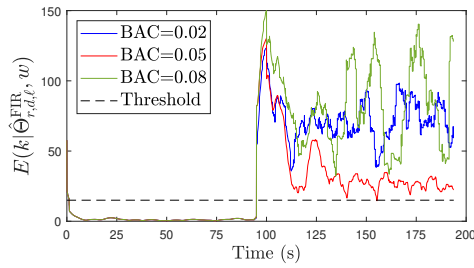


Fig. 9: VISSIM simulation results: Norm of the residuals of the transmissibility operator that relates  $v_2, v_4$  with  $v_3$  computed using (35) with  $w = 100$  steps. The jump in the level of  $E$  above the threshold limits around time  $t = 100$  seconds indicates that abnormal driving conditions are detected.

parameters shown in Table III, and the healthy driver behavior was recorded for the first 100 seconds of the simulations. The identified parameters  $\hat{\Theta}_{r,d}^{\text{FIR}}$  (Markov parameters) of the transmissibility operator that relates the output subset  $v_2, v_4$  to  $v_3$  are plotted in Figure 8a. To validate the identified transmissibility first before implementing the drunk driver detection, we use the identified parameters in Figure 8a along with the measurements of  $v_2, v_4$  to estimate  $v_3$ . The measured velocity  $v_3$  and its transmissibility-based estimation  $\hat{v}_3$  are plotted in Figure 8b.

Next, we modify the human-driver behavior in three separate runs to simulate the drunkenness driving conditions at three different levels as shown in Table III. To observe the norm of residuals, we compute  $E$  using (35) with  $w = 100$  samples as in Figure 6 along with their thresholds using (36). The jump in the level of the norm of residuals above the threshold limits at time  $t = 100$  seconds in Figure 6 indicates that abnormal driving conditions are detected.

## VII. EXPERIMENTAL RESULTS ON ONE HUMAN-DRIVEN ROBOT

Autonomous vehicles are robotics applications that consist of actuators, gross mass, sensors, and closed-loop tracking control. To test the proposed technique experimentally, the experimental setup shown in Figure 10 is used. This setup

consists of three autonomous laboratory robots manufactured by Quanser called Qbot 2e. Qbot 2e is a differential mobile robot that extracts control commands based on an internal inverse kinematics controller. Similar to any other differential robot, two control commands are generated from the controller separately to drive each of the two axial wheels. The angular motion of the differential robots is achieved by setting different velocities for each wheel. We construct the setup by setting the desired velocity of the first robot to Gaussian noise. The second robot is controlled remotely by a human to follow the first robot with level 0 automation. The third robot tracks the velocity of the second robot which is measured through an onboard depth sensor in the third robot. Moreover, the third robot receives the velocity signal of the first robot using a V2V communication link.

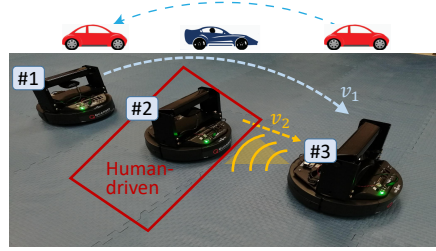


Fig. 10: The first experimental setup: The first robot receives the excitation signal from a computer through a wireless connection. The second robot is human-driven through the computer keyboard. The third robot receives the first robot velocity  $v_1$  via V2V communication and measures the second robot velocity  $v_2$  using an onboard depth sensor.

One-dimensional motion of the setup is considered to characterize the longitudinal motion of the platoon. This is done by setting the velocities of both wheels in the same robot to equal each other. Define two transmissibility operators, the first is  $\mathcal{T}_1$  from  $v_1$  to  $v_2$ , and the second is  $\mathcal{T}_3$  from  $v_3$  to  $v_2$ . Both operators are identified as in Section IV-B. The identified parameters  $\hat{\Theta}_{r,d}^{\text{FIR}}$  (Markov parameters) of both transmissibilities  $\mathcal{T}_1, \mathcal{T}_3$  are plotted in Figure 11a. To validate the identified transmissibilities first before implementing the drunk driver detection, we use the identified parameters of the operator  $\mathcal{T}_1$  in Figure 11a along with the measurements of  $v_1$  to estimate  $v_2$ . The measured velocity  $v_2$  and its transmissibility-based estimation  $\hat{v}_2$  are plotted in Figure 11b. To experience the drunk driver behavior, the effects of BAC= 0.05 shown in Table I were simulated to the interface of the second robot. The reduced coordination and decline in the visual functions are simulated by adding parameters uncertainties to the second robot model. The reduced ability to track moving objects is added as a delay in the human command that is sent from the human to the robot. To simulate the slower response, an equivalent damping was added to the controller of the second robot to yield a higher settling time. To observe the norm of residuals, we compute  $E$  using (35) with  $w = 100$  samples as in Figure 12 along with their thresholds using (36). The jump in the level of the norm of residuals above the threshold limits at time  $t = 50$  seconds in Figure 6 indicates that abnormal

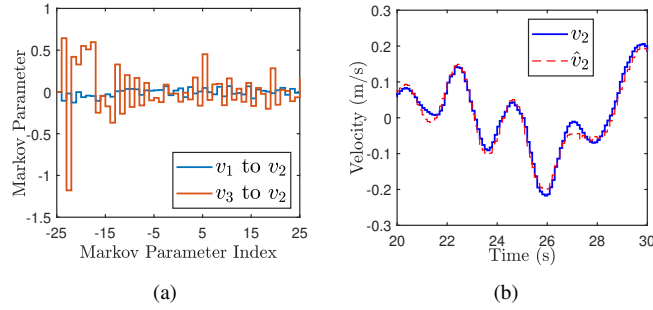


Fig. 11: Experiment 1 results: (a) The identified parameters  $\hat{\Theta}_{r,d}^{\text{FIR}}$  (Markov parameters) of the transmissibility operators  $\mathcal{T}_1, \mathcal{T}_3$  used in the first experiment, and (b) A comparison between the measurements of the velocity  $v_2$  and its transmissibility-based estimation  $\hat{v}_2$ . The estimation of  $\hat{v}_2$  is obtained by implementing the identified transmissibility parameters of  $\mathcal{T}_1$  in Figure 11a along with the measurements of  $v_1$ .

driving conditions are detected.

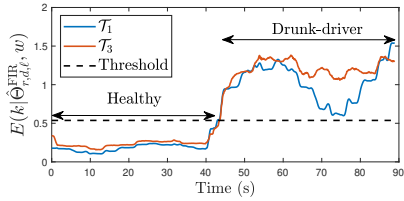


Fig. 12: Experiment 1 results: Norm of the residuals of the transmissibility operators  $\mathcal{T}_1, \mathcal{T}_3$  used in the first experiment computed using (35) with  $w = 100$  steps. The jump in the level of  $E$  above the threshold limits around time  $t = 50$  seconds indicates that abnormal driving conditions are detected.

## VIII. EXPERIMENTAL RESULTS ON TWO HUMAN-DRIVEN ROBOTS

In the previous experiment, only one human-driven robot is considered, and the robot that follows the human-driven is autonomous. In this experiment, we consider the robot that follows the human-driven robot to be another human-driven robot as shown in Figure 13. In this case, the velocity of the first human-driven robot cannot be measured, and it is not accessible for CAVs. The first and fourth robots in the setup shown in Figure 13 are connected autonomous robots same as the robots used in the previous experiment. The second and third robots are human-driven with Level 0 Automation, each is driven by a different human through separate keyboards. The fourth robot receives the velocity of the first robot through a V2V link and measures the velocity of the third robot through an onboard depth sensor. The velocity of the second robot is unknown.

Similar to the first experiment, one dimensional motion of the setup is considered to characterize the longitudinal motion of the platoon. The desired velocity of the first robot is set to Gaussian noise. We construct one transmissibility operator with the pseudo inputs  $y_i = [v_1 \ v_4]$ , to the output  $v_3$ . This transmissibility operator is identified with  $r = 25$  and  $d = 25$ , and the estimated Markov parameters  $\hat{\Theta}_{r,d}^{\text{FIR}}$  are shown in

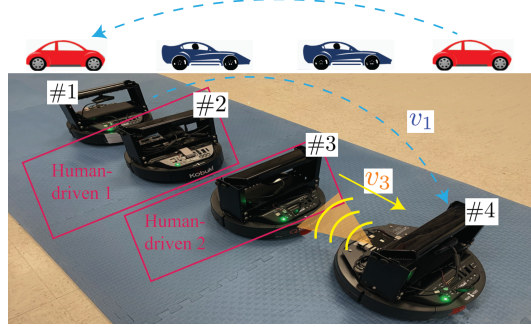


Fig. 13: The second experimental setup: The first robot receives the excitation signal from a computer through a wireless connection. The second and third robots are human-driven through the computer keyboard. The fourth robot receives the first robot velocity  $v_1$  via V2V communication and measures the third robot velocity  $v_3$  using an onboard depth sensor. The velocity of the second robot is unmeasured and inaccessible for the autonomous robots.

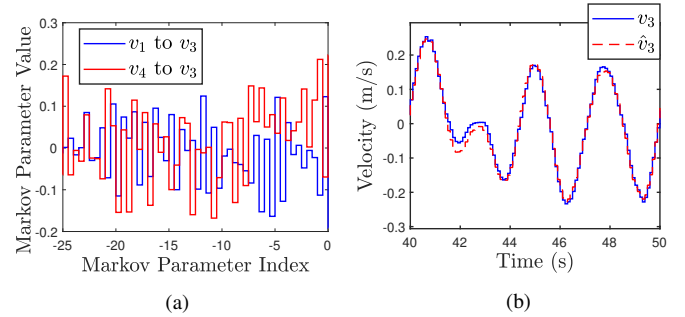


Fig. 14: Experiment 2 results: (a) The identified parameters  $\hat{\Theta}_{r,d}^{\text{FIR}}$  (Markov parameters) of the transmissibility operator from  $v_1, v_4$  to  $v_3$  used in the second experiment, and (b) A comparison between the measurements of the velocity  $v_3$  and its transmissibility-based estimation  $\hat{v}_3$ . The estimation of  $\hat{v}_3$  is obtained by implementing the identified transmissibility parameters in Figure 14a along with the measurements of  $v_1, v_4$ .

Figure 14a. To validate the identified transmissibilities, we use the identified parameters in Figure 14a along with the measurements of  $v_1, v_4$  to estimate  $v_3$ . The measured velocity  $v_3$  and its transmissibility-based estimation  $\hat{v}_3$  are plotted in Figure 14b. The drunk driver effects are simulated as in the previous experiment in the third robot first, then in the second robot at BAC= 0.02, BAC= 0.05, and BAC= 0.08 in each robot within six separate experiments. Figure 15 shows the norm of the residuals of these six experiments computed using (35) between  $v_3$  and  $\hat{v}_3$  with  $w = 100$  steps. From Figure 15, the drunk drivers in both human-driven robots are detected at different levels of intoxication. Note that the case of both human drivers is monitored through  $v_3$  and without the need for  $v_2$ . However, the detection algorithm indicates that a drunk driver is detected or not. Localizing the drunken driver is considered as a future work.

## IX. CONCLUSIONS AND FUTURE WORK

This paper proposed a novel approach for detecting abnormal driver behavior, and more specifically, drunk drivers in platoons with mixed autonomous and human-driven vehicles. The human-driven vehicle was assumed to be between two

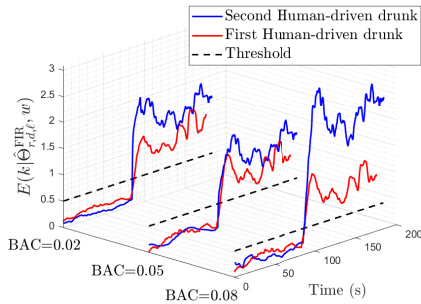


Fig. 15: Experiment 2 results: Norm of the residuals of the transmissibility operators  $\mathcal{T}_1, \mathcal{T}_3$  used in the first experiment computed using (35) with  $w = 100$  steps. The health of both human drivers is monitored through  $v_3$  and its transmissibility-based prediction  $\hat{v}_3$  and without the need for  $v_2$ .

autonomous vehicles, where the autonomous vehicles have the ability to share information through V2V communication links. The proposed approach uses measurements from sensors available on board. The proposed approach was shown to be able to handle the unknown desired velocity of the platoon, unknown normal human-driver behavior, unknown underlying dynamics, and robust against external disturbances. The detectors in the proposed approach are different from the risky vehicle, which gives the ability to the other vehicles to avoid the drunk driver and contact the authorities. We showed that the proposed approach can detect drunk driving behavior with different blood alcohol concentration levels, including relatively low intoxication levels, considering tests based on simulated models of drunk drivers' behaviors. We adopted the IDM human-driver model as an example of healthy human-driver behavior, then the IDM model was developed to simulate the drunken driving conditions at different blood alcohol concentrations. The proposed approach was tested numerically first on a bond-graph model along with the IDM human-driver model, then simulated using VISSIM software. The bond graph model gave more realistic vehicle dynamics, and VISSIM software gave more realistic road topography. Next, the proposed approach was validated using a platoon of laboratory autonomous robots, and the drunken driving conditions were simulated on one of them. The experiments tested the proposed approach by measuring abnormal human-driven vehicles within a network of connected autonomous robots. Since the proposed approach was shown to deal with various system uncertainties, the approach was able to deal with the drunk driver case as well.

The future work is represented in three directions: (i) Develop an algorithm to localize which human driver is drunk in case of multi consecutive human-driven vehicles. Techniques based on machine learning such as techniques used for fault classification as in [37] are proposed to localize which human driver is the drunk one in such cases. (ii) Extend the current approach to investigate its performance on other risky driving behaviors such as distracted or exhausted drivers, and determine what is the best action in each case to ensure road safety. (iii) Extend the current techniques to platoons with more nonlinearities such as platoons with longitudinal

and lateral motion. The longitudinal motion is represented in the vehicle's forward velocity, which was addressed in this work. The lateral motion is represented in the steering, which is considered for future work. This is an important topic when studying drunkenness and driver behaviors. Curved roads such as the road-tested in Section VI-B can be assumed within the unmodeled dynamics  $f$  in equation (7). However, the more complicated road topographies such as urban driving require extending the proposed approach systems with more nonlinearities. A proposed solution for the lateral motion is to consider another set of transmissibilities to count for the lateral motion in parallel with the proposed approach to count for the longitudinal motion.

## REFERENCES

- [1] N. H. T. S. A. (NHTSA), "The effects of blood alcohol concentration," pp. [Online]. Available: <https://www.nhtsa.gov/risky-driving/drunk-driving>.
- [2] P. Chao, M. Cismaru, A. M. Lavack, and E. Markewich, "Social marketing campaigns aimed at preventing drunk driving," *International Marketing Review*, vol. 26, pp. 292–311, 2009.
- [3] R. Berri and F. Osório, "A nonintrusive system for detecting drunk drivers in modern vehicles," in *Brazilian Conference on Intelligent Systems (BRACIS)*, pp. 73–78, São Paulo, Brazil, 2018.
- [4] Y. Feng and M. Wang, "Study on the application of drunk driving detection device design in traffic safety," in *Resilience and Sustainable Transportation Systems*. American Society of Civil Engineers Reston, VA, pp. 134–139, 2020.
- [5] W. Zhao, A. Wang, S. Zou, and H. Zhang, "Individual auxiliary and fault-tolerant control of steer-by-wire system considering different drivers steering characteristics," *IEEE/ASME Transactions on Mechatronics*, 2020.
- [6] A. Bisoffi, F. Biral, M. Da Lio, and L. Zaccarian, "Longitudinal jerk estimation of driver intentions for advanced driver assistance systems," *IEEE/ASME Transactions on Mechatronics*, vol. 22, pp. 1531–1541, 2017.
- [7] X. Liu and P. Kumar, "Towards safety of transportation systems with a mixture of automated and human-driven vehicles," in *International Conference on Communication Systems and Networks (COMSNETS)*, pp. 1–3, 2016.
- [8] D. L. Strayer, F. A. Drews, and D. J. Crouch, "A comparison of the cell phone driver and the drunk driver," *Human factors*, vol. 48, pp. 381–391, 2006.
- [9] E. Haile, "Drunk driver detection system," 1987, US Patent 4,716,413.
- [10] J. Dai, J. Teng, X. Bai, Z. Shen, and D. Xuan, "Mobile phone based drunk driving detection," in *International Conference on Pervasive Computing Technologies for Healthcare*, pp. 1–8, Munich, Germany, 2010.
- [11] K. Murata, E. Fujita, S. Kojima, S. Maeda, Y. Ogura, T. Kamei, T. Tsuji, S. Kaneko, M. Yoshizumi, and N. Suzuki, "Noninvasive biological sensor system for detection of drunk driving," *IEEE transactions on information technology in biomedicine*, vol. 15, pp. 19–25, 2010.
- [12] J. Carroll, D. Bellehumeur, and C. Carroll, "System and method for detecting and measuring ethyl alcohol in the blood of a motorized vehicle driver transdermally and non-invasively in the presence of interferents," 2016, US Patent 9,326,713.
- [13] P. N. Kathar and D. Bhuyar, "Design and implementation of driver drowsiness and alcohol intoxication detection using raspberry pi," *International Journal of Innovative Research in Computer and Communication Engineering*, vol. 4, pp. 617–625, 2016.
- [14] C. Lv, H. Wang, D. Cao, Y. Zhao, D. J. Auger, M. Sullman, R. Matthias, L. Skrypczuk, and A. Mouzakitis, "Characterization of driver neuromuscular dynamics for human–automation collaboration design of automated vehicles," *IEEE/ASME Transactions on Mechatronics*, vol. 23, pp. 2558–2567, 2018.
- [15] M. M. Shirazi and A. B. Rad, "Detection of intoxicated drivers using online system identification of steering behavior," *IEEE Transactions on Intelligent Transportation Systems*, vol. 15, pp. 1738–1747, 2014.
- [16] J. Hu, X. Zhang, and S. Maybank, "Abnormal driving detection with normalized driving behavior data: a deep learning approach," *IEEE Transactions on Vehicular Technology*, vol. 69, pp. 6943–6951, 2020.

- [17] H. Harkous and H. Artail, "A two-stage machine learning method for highly-accurate drunk driving detection," in *International Conference on Wireless and Mobile Computing, Networking and Communications (WiMob)*, pp. 1–6, Barcelona, Spain, 2019.
- [18] A.-T. Nguyen, C. Sentouh, and J.-C. Popieul, "Sensor reduction for driver-automation shared steering control via an adaptive authority allocation strategy," *IEEE/ASME Transactions on Mechatronics*, vol. 23, pp. 5–16, 2017.
- [19] D. I. Katzourakis, N. Lazic, C. Olsson, and M. R. Lidberg, "Driver steering override for lane-keeping aid using computer-aided engineering," *IEEE/ASME Transactions on Mechatronics*, vol. 20, pp. 1543–1552, 2015.
- [20] F. Guedé-Fernandez, M. Fernandez-Chimeno, J. Ramos-Castro, and M. A. Garcia-Gonzalez, "Driver drowsiness detection based on respiratory signal analysis," *IEEE Access*, vol. 7, pp. 81 826–81 838, 2019.
- [21] K. Fujiwara, E. Abe, K. Kamata, C. Nakayama, Y. Suzuki, T. Yamakawa, T. Hiraoka, M. Kano, Y. Sumi, F. Masuda *et al.*, "Heart rate variability-based driver drowsiness detection and its validation with eeg," *IEEE transactions on biomedical engineering*, vol. 66, no. 6, pp. 1769–1778, 2018.
- [22] J. Yu, S. Park, S. Lee, and M. Jeon, "Driver drowsiness detection using condition-adaptive representation learning framework," *IEEE transactions on intelligent transportation systems*, vol. 20, no. 11, pp. 4206–4218, 2018.
- [23] W. Deng and R. Wu, "Real-time driver-drowsiness detection system using facial features," *IEEE Access*, vol. 7, pp. 118 727–118 738, 2019.
- [24] N. N. Charniya and V. R. Nair, "Drunk driving and drowsiness detection," in *2017 International Conference on Intelligent Computing and Control (I2C2)*. IEEE, 2017, pp. 1–6.
- [25] S. Baldi, D. Liu, V. Jain, and W. Yu, "Establishing platoons of bidirectional cooperative vehicles with engine limits and uncertain dynamics," *IEEE Transactions on Intelligent Transportation Systems*, vol. 22, pp. 2679–2691, 2020.
- [26] D. Liu, S. Baldi, V. Jain, W. Yu, and P. Frasca, "Cyclic communication in adaptive strategies to platooning: the case of synchronized merging," *IEEE Transactions on Intelligent Vehicles*, vol. 6, pp. 490–499, 2020.
- [27] K. F. Aljanaideh and D. S. Bernstein, "Time-domain analysis of sensor-to-sensor transmissibility operators," *Automatica*, vol. 53, pp. 312–319, 2015.
- [28] A. Khalil, K. F. Aljanaideh, and M. Al Janaideh, "Output-only measurements for fault detection of multi-actuator systems in motion control applications," *IEEE Sensors Journal*, vol. 22, pp. 4164–4174, 2022.
- [29] A. Khalil, M. Al Janaideh, K. F. Aljanaideh, and D. Kundur, "Fault detection, localization, and mitigation of a network of connected autonomous vehicles using transmissibility identification," in *American Control Conference (ACC)*, pp. 386–391, Denver, CO, 2020.
- [30] J. Monteil and G. Russo, "On the coexistence of human-driven and automated vehicles within platoon systems," in *European Control Conference (ECC)*, pp. 3173–3178, 2019.
- [31] F. Li, D. Mikulski, J. Wagner, and Y. Wang, "Trust-based control and scheduling for UGV platoon under cyber attacks," *SAE Technical Paper*, 2019.
- [32] P. Seiler, A. Pant, and K. Hedrick, "Disturbance propagation in vehicle strings," *IEEE Transactions on Automatic Control*, vol. 49, pp. 1835–1842, 2004.
- [33] M. Treiber, A. Hennecke, and D. Helbing, "Congested traffic states in empirical observations and microscopic simulations," *Physical review E*, vol. 62, pp. 1805–1824, 2000.
- [34] R. H. Middleton and G. C. Goodwin, *Digital Control and Estimation: A Unified Approach*. Prentice Hall PTR, USA, 1990.
- [35] K. F. Aljanaideh and D. S. Bernstein, "Closed-loop identification of unstable systems using noncausal FIR models," *International Journal of Control*, vol. 90, pp. 168–185, 2017.
- [36] A. Youssef, C. Delpha, and D. Diallo, "An optimal fault detection threshold for early detection using kullback–leibler divergence for unknown distribution data," *Signal Processing*, vol. 120, pp. 266–279, 2016.
- [37] A. Khalil and M. Al Janaideh, "On fault classification in connected autonomous vehicles using supervised machine learning," in *IEEE/RSJ International Conference on Intelligent Robots and Systems (IROS)*, pp. 1198–1204, Prague, Czech Republic, 2021.
- [38] A. Khalil, M. Al Janaideh, K. Aljanaideh, and D. Kundur, "Transmissibility-based health monitoring of the future connected autonomous vehicles networks," *IEEE Transactions on Vehicular Technology*, 2022.
- [39] D. C. Karnopp, D. L. Margolis, and R. C. Rosenberg, *System dynamics: modeling, simulation, and control of mechatronic systems*. John Wiley & Sons, 2012.
- [40] L. Zhang and E. Tseng, "Motion prediction of human-driven vehicles in mixed traffic with connected autonomous vehicles," in *American Control Conference (ACC)*, pp. 398–403, Denver, CO, 2020.

## APPENDIX A MIXED PLATOON MODELING

In this appendix, we introduce an analytical bond graph model of the platoon. Although the proposed approach for drunk driver detection does not require knowledge of the platoon, this model is used to numerically apply the proposed approach of drunk driver detection to a model of the mixed platoon.

### A. Autonomous Vehicle Modeling Using the Bond Graph Approach

In this section, we model the electric powertrain topology using the bond graph approach as introduced in [38]. The powertrain is considered as a Brushless DC drive Motor that extracts power from the batteries based on the traction control signal. The controller is assumed to be a PI controller to characterize the cruise-control traction with proportional gain  $k_{P,j}$  and integral gain  $k_{I,j}$ . Figure A.1 shows the bond graph model of the vehicle considered, while parameters description and their numerical values are defined in Table A.1. Following the formulation procedure in [39, Chapter 5, Section 5.3], a mathematical model of the electric vehicle shown in Figure A.1 can be developed. For CAV  $j$ , the bond graph model with the closed loop controller shown in Figure A.1 can be interpreted as

$$\ddot{v}_j(t) + \alpha_j \ddot{v}_j(t) + \beta_j \dot{v}_j(t) + \gamma_j v_j(t) = \delta_j \dot{v}_j^*(t) + \gamma_j v_j^*(t). \quad (\text{A.1})$$

where  $\alpha_j = \kappa_j R_j [\eta_j + 1 + \frac{F_j I_j}{R_j}]$ ,  $\beta_j = \kappa_j [\frac{Q_j^2 \eta_j}{S_j} + F_j + \zeta_j k_{I,j}]$ ,  $\gamma_j = \kappa_j \zeta_j$ ,  $\delta_j = \gamma_j k_{I,j}$ ,  $\kappa_j = \frac{1}{I_j(\eta_j+1)}$ , and  $\zeta_j = \frac{Q_j k_{P,j}}{k_{I,j} G_j r_j M_j}$ .

### B. CAV Platoon with a Human-driven Vehicle

The communication topology shown in [40] is considered as in Figure 2. This topology considers the vehicle in front of the human-driven vehicle to communicate with only the vehicle that follows the human-driven vehicle. The minimal communication links that can be available are used in this paper. Any additional communications (e.g. V2V with the second vehicle that follows the human-driven vehicle and V2C) can be used along with the proposed approach as redundant detectors. Note that if the distance between vehicles  $i_{H-1}$  and  $i_{H+1}$  is longer than the V2V communication range, then this platoon

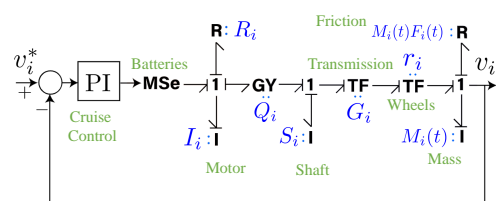


Fig. A.1: Bond graph model of an electric powertrain vehicle that is considered to characterize CAVs.

TABLE A.1: Simulation parameters of the platoon model.

Symbol	Description	Value
$R_j$	Motor Resistance	$18m\Omega$
$I_j$	Motor Inductance	$252\mu H$
$Q_j$	Motor Constant	$0.26\text{rad}/s.A$
$S_j$	Shaft moment of inertia	$0.2kg.m^2$
$G_j$	Transmission Ratio	0.2
$r_j$	Wheel Radius	$0.3m$
$M_j$	Vehicle gross mass	$1478kg$
$F_j$	Friction coefficient	0.6
$k_{P,j}$	Controller proportional gain	2.5
$k_{I,j}$	Controller integral gain	0.6
$\alpha_j$	Constant in (A.1)	72.01
$\beta_j$	Constant in (A.1)	117.9
$\gamma_j$	Constant in (A.1)	46.72
$\delta_j$	Constant in (A.1)	28.03
$a_{\max}$	Maximum acceleration in (1)	$1m/s^2$
$\lambda$	Constant in (1)	4
$s_0$	Minimum spacing distance in (2)	$2m$
$T$	Time constant in (2)	1.5 seconds

is considered two separate fully autonomous platoons. CAV vehicles send information regarding the position, velocity, and acceleration to the following vehicle via V2V communication links. According to [40], CAV  $i_H + 1$  receives the information  $[ s_{i_H-1} \ v_{i_H-1} \ a_{i_H-1} ]^T$  via the V2V communication link. Moreover, vehicle  $i_H + 1$  measures  $[ s_{i_H} \ v_{i_H} \ a_{i_H} ]^T$  using the perception sensors such as radar and LiDAR. For all  $j \in \{1 \dots n\} \setminus \{i_H + 1\}$  the  $j$ th vehicle uses the velocity of the preceding vehicle as the desired velocity, that is,  $v_j^* = v_{j-1}$ . To avoid collision between the human-driven vehicle and the succeeding vehicle (i.e. vehicle  $i_H + 1$ ), the desired velocity of vehicle  $i_H + 1$  is set as

$$v_{i_H+1}^*(t) = \begin{cases} \frac{v_{i_H}(t) + v_{i_H-1}(t)}{2}, & v_{i_H+1} < v_{i_H}, \\ v_{i_H}(t), & v_{i_H+1} \geq v_{i_H}, \end{cases} \quad (\text{A.2})$$

that is, if the human-driven vehicle is faster than vehicle  $i_H + 1$ , then vehicle  $i_H + 1$  follows the average of the velocities of the two preceding vehicles. Otherwise, vehicle  $i_H + 1$  follows only the velocity of vehicle  $i_H$ . Next, for all  $t \geq 0$ , let  $u(t) = v_1^*(t)$ ,  $y(t) = [ v_1(t) \ \dots \ v_n(t) ]^T$  and consider the condition  $v_{i_H+1} < v_{i_H}$  is satisfied for all  $t$ . The a mixed platoon of  $n$  vehicles, where vehicle  $i_H$  is human-driven can be represented using the state space equations (7)-(8) where

$$A = \begin{bmatrix} A_1 & & \dots & 0 \\ B_2 C_1 & \ddots & & \vdots \\ \vdots & \ddots & A_{n-1} & 0 \\ 0 & & B_n C_{n-1} & A_n \end{bmatrix}, \quad (\text{A.3})$$

$$B_v = [ B_1 \ 0 \ \dots \ 0 ]^T, \quad (\text{A.4})$$

$$B_f = [ 0 \ \dots \ 0 \ 1 \ 0 \ \dots \ 0 ]^T, \quad (\text{A.5})$$

$$C = \text{diag}(C_1, \dots, C_n). \quad (\text{A.6})$$

For all  $j \in \{1, \dots, n\} \setminus \{i_H\}$ ,  $A_j$ ,  $B_j$  and  $C_j$  are given by

$$A_j = \begin{bmatrix} 0 & 1 & 0 \\ 0 & 0 & 1 \\ -\gamma_j & -\beta_j & -\alpha_j \end{bmatrix}, \quad B_j = \begin{bmatrix} 0 \\ \delta_j \\ \gamma_j - \alpha_j \delta_j \end{bmatrix},$$

$$C_j = [ 1 \ 0 \ 0 ].$$

Without any loss of generality, the human-driven vehicle

acceleration  $a_{i_H}$  can be written as

$$\begin{aligned} \dot{x}_{i_H}(t) &= a_{i_H}(t, x_{i_H}) \\ &= A_{i_H} x_{i_H}(t) + B_{i_H} C_{i_H-1} x_{i_H-1}(t) + f(t, x), \end{aligned} \quad (\text{A.7})$$

such that the human behavior is split into a linear and nonlinear parts. The IDM model in (1) is used to obtain the measurements of the state  $x_{i_H} = v_{i_H}$ , however,  $A_{i_H}$ ,  $B_{i_H}$ , and  $f$  are assumed to be unknowns. We also consider the rest of the platoon model (7)-(8) to be unknown and only the outputs  $y(t)$  are measured from the bond graph model.



**Abdelrahman Khalil** received the B.Sc. degree in Aeronautical Engineering from Jordan University of Science and Technology, Irbid, Jordan in 2018. He is currently a Ph.D. candidate in Mechanical Engineering at Memorial University of Newfoundland, St. John's, Canada. His research interests include adaptive estimation theory, fault detection and diagnosis, fault-tolerant control, and system identification.



**Khaled Aljanaideh** received the B.Sc. degree in mechanical engineering (top of class) from Jordan University of Science and Technology, Irbid, Jordan in 2009. He also received the M.S.E. and M.Sc. degrees in aerospace engineering and applied mathematics and the Ph.D. degree in aerospace engineering all from the University of Michigan, Ann Arbor, in 2011, 2014, and 2015, respectively. He is an assistant professor in the Department of Aeronautical Engineering, Jordan University of Science and Technology. He was a postdoctoral research fellow in the Department of Aerospace Engineering at the University of Michigan between 2015 and 2016, where he also was a part time visiting assistant professor between 2017 and 2019. He is currently with The MathWorks, Natick, MA. His current research interests are in system identification and fault detection for aerospace and mechanical systems.



**Mohammad Al Janaideh** received the M.A.Sc. and Ph.D. degrees in mechanical engineering (mechatronics and control) from Concordia University, Canada, in 2005 and 2010, respectively. He was a Postdoctoral Fellow with the Department of Electrical and Computer Engineering, University of Toronto, and the Department of Aerospace Engineering, University of Michigan, Ann Arbor. He also worked as a Senior Mechatronics Engineer at ASML, CT, USA. Since 2017, he has been with the Department of Mechanical Engineering, Memorial University of Newfoundland, Canada. His research interests include design and control of micro- and nano-positioning systems, fault detection and mitigation of connected autonomous robotics networks, design and control of precision motion stages for semiconductor manufacturing machines, and control of systems with uncertain hysteresis nonlinearities. He is a Technical Editor of IEEE Transactions on Mechatronics, IEEE Conference of Decision and Control (CDC), and the American Control Conference (ACC).